american physiological society
JOURNAL OF APPLIED PHYSIOLOGY

J Appl Physiol 139: 849–862, 2025.
First published August 27, 2025; doi:10.1152/japplphysiol.00377.2025

RESEARCH ARTICLE

Biomechanical implications of mass loading in a swine model of acute hypoxemic respiratory failure

Alice Nova,[1] Yi Xin,[1] Marcus Victor,[1] Timothy G. Gaulton,[1] Glasiele C. Alcala,[1] Tilo Winkler,[1] Sarah E. Gerard,[2] Rehab Khalid,[3] Rajiv Gupta,[3] Emanuele Rezoagli,[4,5] Lorenzo Berra,[1] Marcelo B. P. Amato,[6,7] Jason H. T. Bates,[8] and Maurizio Cereda[1]

[1]*Anesthesia Center for Critical Care Research, Department of Anaesthesiology, Critical Care and Pain Medicine, Mass General Brigham and Harvard Medical School, Boston, Massachusetts, United States;* [2]*Roy J. Carver Department of Biomedical Engineering, The University of Iowa, Iowa City, Iowa, United States;* [3]*Department of Radiology, Mass General Brigham and Harvard Medical School, Boston, Massachusetts, United States;* [4]*Department of Emergency and Intensive Care, Fondazione IRCCS San Gerardo dei Tintori, Monza, Italy;* [5]*School of Medicine and Surgery, University of Milano-Bicocca, Monza, Italy;* [6]*Divisão de Pneumologia, Faculdade de Medicina da Universidade de São Paulo, São Paulo, Brazil;* [7]*Instituto do Coração, Hospital das Clinicas, Faculade de Medicina da Universidade de São Paulo, São Paulo, Brazil; and* [8]*Pulmonary/Critical Care Division, Department of Medicine, University of Vermont, Burlington, Vermont, United States*

Abstract

In obesity, excess weight of the chest and abdomen (mass loading) decreases lung volume and can worsen acute hypoxemic respiratory failure (AHRF). We investigated whether positive end-expiratory pressure (PEEP) fully reverses the effects of mass loading on lung volume and respiratory mechanics in an AHRF swine model. Eighteen Yorkshire pigs were studied: six healthy, eight pre- and postinjury, and four postinjury only. We randomly tested three mass loading conditions: without mass loading, with abdominal loading (6 kg weight), and with combined abdominal and chest mass loading (12 kg total weight). We performed a recruitment maneuver in each condition, followed by a decremental PEEP trial, and identified the best-PEEP as that with the greatest respiratory system compliance (C_{RS}). Airway pressure, esophageal pressure, and thoracic impedance by electrical impedance tomography) were continuously monitored. After lung injury, best-PEEP increased with loading. C_{RS} at best-PEEP decreased from 20.6 ± 3.4 mL/cmH_2O without loading to 17.7 ± 3.0 mL/cmH_2O with abdominal loading [mean difference 2.9, 95% confidence interval (CI): 1.6–4.2] and to 14.2 ± 2.8 mL/cmH_2O with abdominal and chest loading (mean difference 6.3, 95% CI: 5.0–7.7). Any amount of loading decreased end-expiratory lung volume assessed by computed tomography (CT) at best-PEEP and PEEP 3 cmH_2O. Combined abdominal-chest loading decreased the vertical lung dimension on CT compared with unloaded and abdominal loading at both levels of PEEP. With mass loading, PEEP did not restore values of C_{RS} and lung aeration to their unloaded values. In AHRF with mass loading, geometrical constraints may limit PEEP efficacy even when optimally titrated.

NEW & NOTEWORTHY In a ventilated swine model, we isolated the mechanical effects of mass loading from those of lung injury. Despite optimization, positive end-expiratory pressure (PEEP) could not restore baseline pulmonary compliance or lung volumes in either healthy or injured lungs. Partitioned respiratory mechanics and imaging reveal that geometric constraints and load-induced airway closure, demonstrated here for the first time in injured swine, may limit the effectiveness of recruitment maneuvers and optimized PEEP in mass-loaded lungs.

acute hypoxemic respiratory failure; mechanical ventilation; obesity

INTRODUCTION

Obesity increases disease severity and morbidity in acute hypoxemic respiratory failure (AHRF) (1–3). Excess adiposity, when located in the abdomen and chest, compresses the lung and impairs respiratory mechanics (4). Individualized positive end expiratory pressure (PEEP) titration, a key treatment in AHRF, may not reverse the effects of excess adiposity on respiratory mechanics (5). Unfortunately, there is little mechanistic evidence to guide ventilation in this population due to their underrepresentation in clinical trials of AHRF and the lack of experimental models that isolate the mechanical consequences of truncal adiposity (6).

Truncal adiposity displaces the diaphragm cephalad and increases intrathoracic pressure (7–9). Elevations in intrathoracic pressure result in airway and alveolar collapse (10) that worsen gas exchange (11) and may complicate assessments of the severity of underlying lung injury. Lung

Correspondence: M. Cereda (mcereda@mgh.harvard.edu).
Submitted 5 May 2025 / Revised 22 June 2025 / Accepted 19 August 2025

collapse may further contribute to secondary lung injury due to uneven ventilation (12, 13) and intermittent reopening of atelectasis (e.g., atelectrauma) (14). Although higher PEEP is often empirically applied to patients with obesity (15, 16), its effect on global and regional respiratory mechanics in the presence of mass loading is unclear. Moreover, adipose tissue distribution is variable (17), as described by anthropometric indices (18, 19), for a given body mass index, which may further affect respiratory mechanics, responses to PEEP, as well as airway closure, a common phenomenon in AHRF (20).

Addressing these knowledge gaps is crucial to understand how excess adiposity influences disease severity and treatment response. To this end, we developed a ventilated large animal model in which the application of variable mass loads on the abdomen and chest can be superimposed on experimental lung injury. We collected global and topographic measurements of respiratory mechanics and lung morphology to assess how the characteristics of mass loading modify the physiological effects of lung injury and the responses to the application of PEEP.

MATERIALS AND METHODS

The study was approved by the Institutional Animal Care and Use Committee and conducted at Massachusetts General Hospital (Boston, MA) between February and October 2024. A protocol flowchart is shown in Supplemental Fig. S1*A*. Eighteen Yorkshire pigs (average weight 30.6 ± 4.2 kg) were studied: eight before and after lung injury, six in healthy status only, and four after lung injury only (Supplemental Fig. S1*B*).

Animal Preparation and Monitoring

Eighteen Yorkshire 3–4 mo-old pigs were sedated with intramuscular tiletamine/zolazepam 4.4 mg/kg, xylazine 2.2 mg/kg, and atropine 0.04 mg/kg. Anesthesia was induced with fentanyl 2 μg/kg, propofol 2 mg/kg, and pancuronium 0.1 mg/kg, and maintained by intravenous infusion of propofol 10–12 mg/kg/h and fentanyl 10 μg/kg/h. Central venous and arterial catheters were placed in the right internal jugular vein and in the femoral artery, respectively, under ultrasound guidance. Oxygen saturation by pulse oximetry (Sp_{O_2}), heart rate, electrocardiogram, and blood pressure were continuously monitored. The bladder was catheterized for urine output monitoring and intraabdominal pressure measurement. All animals received intravenous hydration with lactated Ringer's solution. Core temperature was monitored and controlled with active surface heaters. All pigs were orally intubated and mechanically ventilated (Servo-i; Maquet, Sweden) in volume-controlled ventilation. PEEP was set to 3 cmH_2O and tidal volume was set between 8 and 10 mL/kg to maintain driving pressure $\leq$14 cmH_2O at baseline. Respiratory rate was set and modified during the experiment to keep pH above 7.25. In the healthy condition, the inspired oxygen fraction (FI_{O_2}) was maintained at 0.4, and increased to 1 after lung injury.

In all animals, an esophageal balloon-catheter (Cooper Surgical, CT) was placed and connected to a dedicated acquisition system (Pneumodrive, Bionica, Brazil). The correct balloon was positioned in the esophagus such that respiratory and cardiac oscillations were evident in esophageal pressure (P_{es}) waveform. If not, the catheter was adjusted—either advanced or withdrawn—while monitoring the P_{es} waveform until cardiac oscillations appeared. We recorded static (P_{es}) and airway pressure (P_{aw}) by airway occlusion maneuvers at end-expiration while the esophageal balloon was progressively inflated from 0 to 8 mL in steps of 0.2 mL using an automatic system (Pneumodrive, Bionica, Brazil). We obtained the relationship between balloon filling volume and P_{es} from these data. A slope of P_{es}/P_{aw} between 0.8 and 1.2 was considered optimal (21, 22). The proper position of the balloon was subsequently confirmed by comparing the swings in P_{aw} (ΔP_{aw}) and P_{es} (ΔP_{es}) generated by chest compression during a manual end-expiratory hold. We considered a range of $0.8 < \Delta P_{es}/\Delta P_{aw} < 1.2$ to be acceptable (i.e., Baydur's test) (23). The catheter was deflated periodically by applying a pressure of -20 cmH_2O and refilled with the optimal volume to avoid biased measurements due to possible leaks. After the measurement of thoracic circumference, an electrical impedance tomography (EIT) belt was positioned at the level of the fourth to sixth rib and connected to the Enlight 2100 EIT (Timpel, Brazil) device. The location of the belt was marked on the skin with a marker. A pneumotachograph was placed proximally to the endotracheal tube and connected to the EIT monitor. P_{aw} and P_{es} were continuously recorded. EIT continuously measured thoracic impedance variations during the respiratory cycle at a rate of 50 Hz.

Lung Injury

Lung injury was induced in 12 animals. After instrumentation and stabilization, the animals received 3.5 mL/kg of hydrochloric acid (HCl, pH 1.0). This was divided into 5-mL aliquots and instilled via bronchoscopy (Ambu Inc.) into the lobar bronchi of each lung to ensure symmetric distribution of the acid. As shown in published studies (24), this protocol induces significant inflammatory lung injury resulting in low respiratory compliance and hypoxemia. We started the study protocol after 2 h of injury stabilization.

Study Protocol

We generated three different conditions of mechanical mass loading by using customized square sandbags: no loading, abdominal loading only (6 kg on the mid-abdomen), and combined abdominal and chest loading (6 kg on the mid-abdomen and 6 kg on the lower chest). The same sandbags were used for all the animals enrolled in the study. The sandbag placed over the abdomen measured ~30 cm × 20 cm × 4 cm, whereas the sandbag placed over the chest measured ~20 cm × 15 cm × 8 cm. The EIT belt was used as a reference to standardize the sandbag placement across all animals and to allow accurate repositioning in case of displacement. The thoracic sandbag was placed 1 cm above the upper edge of the belt, whereas the abdominal sandbag was placed 2 cm below the lower edge. Impedance signal quality was continuously monitored. If the sandbags affected the belt's adherence to the chest surface, compromising signal quality, we corrected it by repositioning the sandbags, applying additional conductive gel, or tightening the belt. All experiments were conducted with verified high-quality impedance signals, as documented by the EIT system. The load conditions were

tested in random order using sealed envelopes containing the sequence written on slips of paper. Between load conditions, after removing the weights, we performed a lung recruitment maneuver in continuous positive airway pressure (CPAP) mode by increasing PEEP in 5 cmH_2O increments every 5–10 s until reaching 40 cmH_2O, which was then sustained for 40 s (16).

For each load condition, arterial blood gases and hemodynamic parameters were collected, followed by a low flow inflation (20, 25) (5 L/min) with an inflation volume of 400 mL starting from PEEP 0, after a prolonged expiration. Then, we performed a second recruitment maneuver (16) followed by a decremental PEEP trial (26) from PEEP 20 to 4 cmH_2O in steps of 2 cmH_2O. The best-PEEP was defined as the level corresponding to the highest respiratory system compliance (C_{RS}).

In four healthy animals and in seven animals with lung injury, computed tomography (CT) scans were performed using a portable CT scanner (NeuroLogica Portable CT Scanner, OmniTom Elite with Photon Counting Detector). For each condition, CT images were acquired during a prolonged expiratory breath hold at PEEP 3 cmH_2O and at the titrated best-PEEP. Each image covered 20 cm along the longitudinal axis of the thorax at 120 kV and 20 mA. The spiral acquisition took ~18 s per scan. The images were reconstructed using a soft-tissue kernel with 0.848 mm isotropic voxel resolution.

Muscle relaxant (pancuronium 0.05 mg/kg) was administered at the beginning of each load condition to avoid spontaneous breathing activity during low flow inflation, respiratory mechanics measurements, and CT scans.

Off-Line Analysis

Respiratory system mechanics.

Transpulmonary pressure was calculated as the difference between P_{aw} and P_{es}. This allowed C_{RS} to be partitioned between the lung (C_L) and chest wall (C_{C_W}) (27) at each PEEP level. The presence of airway closure was assessed off-line by analyzing the recorded airway pressure-volume tracings. Complete airway closure was inferred from the pattern of the pressure-volume curve during low-flow inflation, as described previously (20, 25, 28). Below an inflection point early in the initial part of the curve, when pressure was low, the absence of cardiac oscillations, and a value of C_{RS} close to that of the occluded breathing circuit (between 1.5 and 2.5 mL/cm H_2O) were taken to indicate complete airway closure. Once pressure exceeded the low inflection point, cardiac oscillations became apparent in the airway pressure tracing, and compliance increased abruptly. The low inflection point was thus taken to correspond to the pressure at which the collapsed lung started to inflate, defined as the opening pressure (P_O). Respiratory system driving pressure (ΔP) is conventionally defined as the difference between the inspiratory plateau pressure (P_{plat}) and PEEP, whereas C_{RS} is defined as the ratio of tidal volume (V_T) to ΔP. For pigs in which $P_O > PEEP$, ΔP and C_{RS} were calculated as follows (20):

$$\Delta P = P_{plat} - P_O \tag{1}$$

and

$$C_{RS} = \frac{V_T}{P_{plat} - P_O}. \tag{2}$$

Lung compliance (C_L) was then calculated as:

$$C_L = \frac{V_T}{(P_{plat} - P_O) - \Delta P_{es}}, \tag{3}$$

where ΔP_{es} corresponds to the swing of esophageal pressure from end-inspiration to end-expiration.

CT analysis.

All CT chest images underwent a segmentation process using a previously validated automated deep-learning image analysis pipeline, which comprises a multiresolution unsupervised convolutional neural network (29–31). Quantitative analysis of CT scans was performed using established methods (29–31). For each region of interest, frequency histograms of Hounsfield units (HU) were extracted. These distributions were partitioned among compartments of different aeration: nonaerated (−100 to +100 HU), poorly aerated (−500 to −101 HU), normally aerated (−900 to −501 HU), and hyperinflated (−1,000 to −901 HU). Each compartment was measured as the percentage of the total slice area it occupied (32). The global superimposed pressure (SP_{global}), the hydrostatic pressure exerted by the weight of the lungs across the whole lung, was assessed at the highest anteroposterior section of the lungs, thus:

$$SP_{global} = 1 - \frac{\text{CT numbers (HU)}}{-1.000} h, \tag{4}$$

where the h is the distance (in cm) between the ventral and the dorsal borders of the lung (Fig. 1*A*).

For each scan obtained at each PEEP level, we evaluated the change in lung shape across different load conditions by measuring lung height, width, and length. The maximal lung height was measured on the transverse plane at the level of the carina (lung $height_{CAR}$) and the diaphragm dome (lung

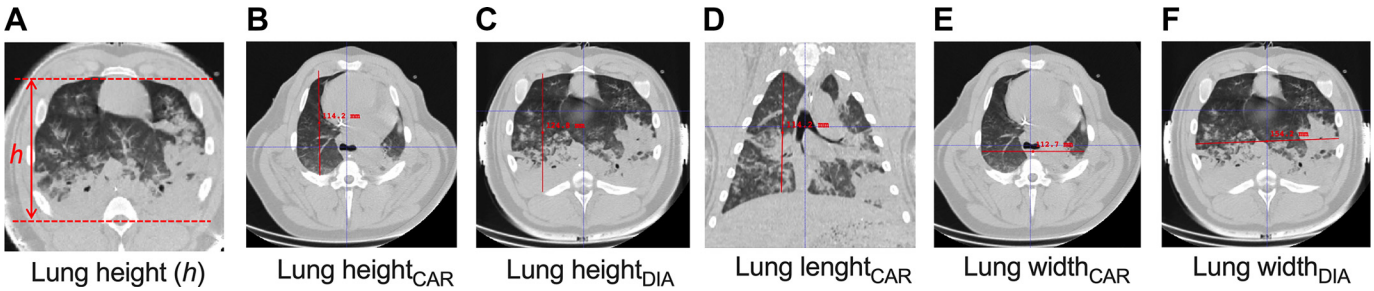

Figure 1. Representative CT with measurements of lung dimensions. *A*: lung height (*h*), distance (cm) between the ventral and the dorsal borders of the lung, used to calculate global superimposed pressure. *B*: $height_{CAR}$, height of the lung at carina level. *C*: $height_{DIA}$, height of the lung at diaphragm level. *D*: $length_{CAR}$, length of the lung at carina level. *E*: $width_{CAR}$, width of the lung at carina level. *F*: $width_{DIA}$, width of the lung at diaphragm level. CT obtained at PEEP 3 cmH_2O at injured and unloaded condition. CT, computed tomography; PEEP, positive pressure at end expiration.

height$_{DIA}$). The maximal lung width was measured on the coronal plane at the level of the carina (lung width$_{CAR}$) and the diaphragm dome (lung width$_{DIA}$). The maximal lung length was then measured on the coronal plane at the carina level (lung length$_{CAR}$). An example of lung shape measurements is provided in Fig. 1, *B–F*. Offline analyses of lung shape were performed using dedicated software (ITK-SNAP, version 3.8.0, University of Pennsylvania and University of Utah).

EIT analysis.

EIT data were acquired using the Enlight EIT device (Timpel, São Paulo, Brazil). Images based on a three-dimensional finite element model were reconstructed, assuming a 6 cm wide cross section of the thorax, and plotted in a matrix containing 860 pixels. EIT maps obtained during decremental PEEP titration were used to record percent values of lung collapse or overdistension as follows (33, 34). First, the compliance, C_i, of each pixel was calculated at each PEEP step according to:

$$C_i = \frac{\Delta Z_i}{\Delta P}; i = 1, \ldots, 860, \quad (5)$$

where ΔZ_i is the impedance variation of the ith pixel. Next, at each PEEP step, the percent change in C_i relative to its maximal value, $C_{i,\max}$, for all PEEP steps provided the percent collapse for that pixel thus:

$$\Delta C_i = 100\left(\frac{C_{i,\max} - C_i}{C_{i,\max}}\right). \quad (6)$$

ΔC_i is set to 0 if the best compliance pixel has not yet been achieved for that pixel. Finally, the cumulative % change in pixel compliance, ΔC, was computed at each PEEP step as the weighted average of the individual collapses for each pixel weighted by its respective maximum compliance thus:

$$\Delta C_w = \frac{\sum_{i=1}^{860} \Delta C_i C_{i,\max}}{\sum_{i=1}^{860} C_{i,\max}}. \quad (7)$$

When ΔC_w was negative, it represented a measure of the degree of lung collapse, whereas when it was positive, it represented a measure of the degree of hyperdistention. Hyperdistention pixel (%) was set to 0 if the best compliance pixel has already been achieved for that pixel.

Statistical Considerations

Normality was assessed by the Shapiro–Wilk test. Continuous data were expressed as means ± SD or median and interquartile range [IQR], as appropriate. Categorical data were expressed as count (proportion). Since each animal was evaluated under three load conditions, we used repeated measures ANOVA analysis, Friedman test or McNemar's test, as appropriate, to examine differences among the different conditions. Multiple comparison was conducted using Tukey's correction method to assess differences in the continuous variables between two different load conditions. We performed the *t* test or Mann–Whitney test, as appropriate, to compare healthy and injured groups within the same load condition. The effects of the interactions of load, PEEP, and presence of injury on continuous variables were tested using three-way ANOVA. Statistical significance was set at $P < 0.05$ (two-tailed). Stata/MP version 17 (StataCorp LLC, College Station, TX) and GraphPad Prism version 10.2.2 (GraphPad Software, Inc., San Diego, CA) were used for the statistical analysis.

Sample Size Justification

Our preliminary studies revealed a medium-to-large effect size on C_{RS} between unloaded and abdominal load conditions (decreasing from 28 ± 4 mL/cmH_2O at unloaded condition to 18 ± 3 mL/mH_2O under abdominal load) at a baseline PEEP of 3 cmH_2O. With a two-sided 0.05 significance level and a power of 0.8, the above difference in C_{RS} between the load conditions gives a minimum required sample size of 8 for the experimental crossover animal model study.

RESULTS

All 18 pigs survived the experiment. Eight out of 18 pigs (46%) were female. Pa_{O_2}/FI_{O_2} was lower in injured versus healthy lungs across all tested conditions: 267 ± 138 mmHg versus 470 ± 70 mmHg in unloaded ($P < 0.001$), 177 ± 114 mmHg versus 424 ± 98 mmHg in abdominal loading ($P < 0.001$), and 139 ± 90 mmHg versus 420 ± 124 mmHg at abdominal and chest loading ($P < 0.001$). Mass loading reduced Pa_{O_2}/FI_{O_2} from unloaded values only in injured lungs ($P < 0.001$). Complete blood gas and hemodynamic data are provided in Supplemental Tables S1 and S2.

Respiratory Mechanics

Mass loading and PEEP increased the end-expiratory P_{es} in healthy (Fig. 2*A*) and injured (Fig. 2*B*) pigs, although end-expiratory esophageal pressure did not differ between abdominal versus combined abdominal and chest loading after injury. Intra-abdominal pressure increased sequentially with mass loading in healthy (Table 1) and injured pigs (Table 2). We did not observe any statistically significant differences in end-expiratory P_{es} between healthy animals and animals with lung injury across any of the load conditions (Supplemental Table S3). However, we observed a trend toward lower end-expiratory P_{es} in pigs with lung injury compared with healthy animals. Figure 3 shows the effects of loading and PEEP on C_{RS} in healthy (Fig. 3*A*) and injured (Fig. 3*B*) lungs. In both healthy and injured animals, load application decreased C_{RS} compared with the unloaded condition up to PEEP of 16 cmH_2O. At higher PEEP levels (e.g., 18–20 cmH_2O), C_{RS} in the unloaded condition began to decrease, showing lower values than those observed in loaded condition ($P < 0.05$). We observed a significative interaction effect of load ($P < 0.001$), PEEP and lung injury on C_{RS}. The best-PEEP increased with load intensity in healthy (Table 1) and injured (Table 2) lungs. In healthy lungs, the mean values of C_{RS} at best-PEEP decreased from 33.9 ± 4.7 without loading to 27.6 ± 3.5 with abdominal loading [mean difference 11.7, 95% confidence interval (CI): 9.1–14.3] and to 22.1 ± 3.8 with abdominal and chest loading (mean difference 5.5, 95% CI: 3.5–7.5). Following injury, the mean C_{RS} at best-PEEP decreased from 20.6 ± 3.4 without loading to 17.7 ± 3.0 with abdominal loading (mean difference 2.9, 95% CI: 1.6–4.2) and to 14.2 ± 2.8 with abdominal and chest loading (mean difference 6.3, 95% CI: 5.0–7.7). C_L followed similar trends to C_{RS} across PEEP levels in both

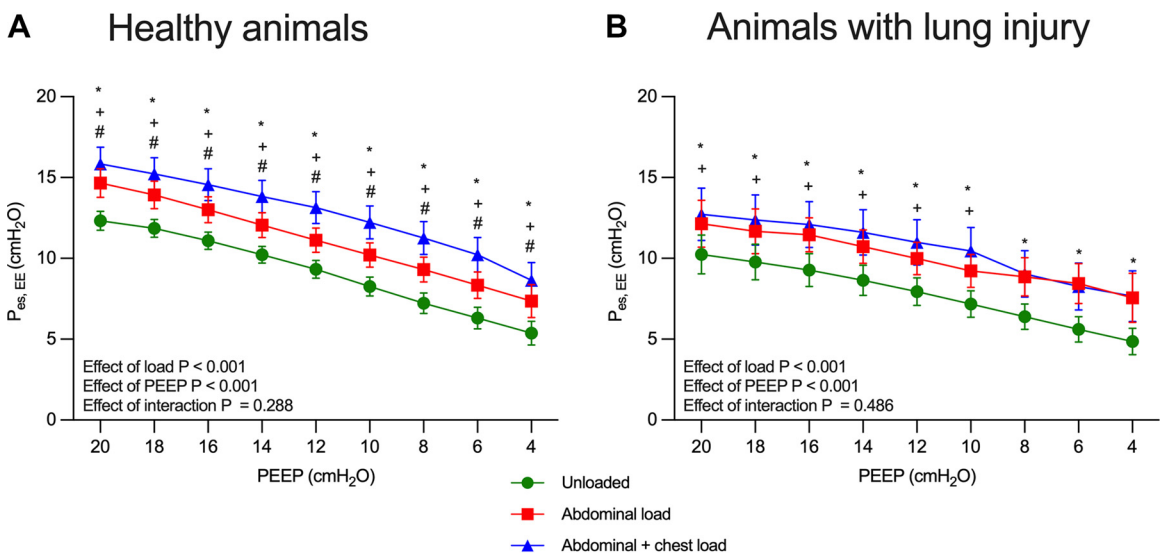

Figure 2. Esophageal pressure at end-expiration in healthy pigs (*A*) and in pigs with lung injury (*B*). $n = 14$ (healthy animals); $n = 12$ (injured animals); data are presented as means ± SE; *P* for repeated measured ANOVA; green circles indicate the unloaded condition, red squares indicate the abdominal load condition, and blue triangles indicate the combined abdominal + chest load condition; $*P < 0.05$ for comparison between unloaded and abdominal load; $+P < 0.05$ for comparison between unloaded and abdominal + chest load; $\#P < 0.05$ for comparison between abdominal load and combined abdominal + chest load. PEEP, positive pressure at end expiration; $P_{es, EE}$, esophageal pressure at end-expiration.

healthy (Table 1, Fig. 4*A*) and injured (Table 2, Fig. 4*B*) lungs. C_{C_W} was minimally affected by loading (Fig. 4).

Computed Tomography

Figures 5 and 6 show representative CT images of healthy and injured lungs, respectively, demonstrating a loss of aeration with loading at both low PEEP and best-PEEP levels. This effect was more pronounced in the injured lungs. Quantitative CT analysis revealed that load application increased the volume of nonaerated tissue, particularly in the dorsal lung regions at low PEEP, in both healthy (Fig. 7) and injured lungs (Fig. 8). The best-PEEP attenuated but did not eliminate the effect of loading on aeration distribution.

In injured lungs, both abdominal loading and combined abdominal and chest loading reduced end-expiratory lung volume (EELV) relative to no loading (Fig. 9*A*) at low PEEP, whereas at best-PEEP, the effect was statistically significant only for combined abdominal and chest loading. A plot of C_{RS} versus EELV (Fig. 9*B*) shows that, moving from PEEP 3 cmH_2O to the best-PEEP, both EELV and C_{RS} increased to values that were lower in loaded than in unloaded conditions. In abdominal loading, the C_{RS} versus EELV relationship was similar to when no loading was present. However, abdominal and chest loading resulted in lower C_{RS} values compared with no loading at equivalent EELV (Fig. 9*B*, dashed line). EELV and the C_{RS} versus EELV plots in healthy lungs are shown in Supplemental Fig. S2. After injury, load application reduced the height of the lung (at the diaphragm and carina) and its length at both low PEEP (Supplemental Fig. S3*A*) and best-PEEP (Supplemental Fig. S3*B*), with a statistically significant effect of chest loading on lung height. No significant differences in lung width were observed. Similar trends were observed in healthy pigs (Supplemental Fig. S4). SP_{global} (*Eq. 4*) is shown for healthy (Supplemental Fig. S5*A*) and injured (Supplemental Fig. S5*B*) lungs. Its values increased with lung injury ($P < 0.001$) and decreased with best-PEEP in all load conditions and in both injured and healthy lungs ($P < 0.05$). Loading caused a rise in SP_{global} that was statistically significant only in the injured lungs.

Table 1. *Respiratory mechanics parameters in healthy animals*

Parameter	Unloaded	Abdominal Load	Abdominal + Chest Load	Estimated Mean Difference (95% CI)		
				Unloaded vs. Abdominal Load	Unloaded vs. Abdominal + Chest Load	Abdominal vs. Abdominal + Chest Load
Best-PEEP, cmH_2O	7.9 ± 1.3	11.8 ± 1.5	14.1 ± 2.4	−3.9 (−4.7 to −3.1)	−6.4 (−7.9 to −4.9)	−2.3 (−3.6 to −0.9)
Best-C_{RS}, mL/cmH_2O	33.9 ± 4.7	27.6 ± 3.5	22.1 ± 3.8	6.2 (4.2 to 8.2)	11.7 (9.1 to 14.3)	5.5 (3.5 to 7.5)
C_{RS} PEEP3, mL/cmH_2O	31.0 ± 4.1	20.0 ± 2.8	15.5 ± 3.1	11.1 (9.7 to 12.5)	14.7 (12.6 to 16.8)	4.5 (2.5 to 6.5)
Best-C_L, mL/cmH_2O	70.0 [56.5–94.0]	47.0 [32.0–63.0]	32.0 [25.0–38.0]	24.1 (13.4 to 34.8)	35.9 (25.5 to 46.3)	14.1 (4.9 to 23.3)
C_L PEEP3, mL/cmH_2O	59.0 [42.0–67.0]	29.0 [24.5–40.5]	23.0 [19.0–42.0]	20.5 (14.5 to 26.5)	26.1 (18.0 to 34.2)	5.3 (1.1 to 9.4)
Best-$PEEP_{CP}$, mL/cmH_2O	8.3 ± 1.5	13.9 ± 1.7	15.6 ± 1.9	−5.6 (−6.6 to −4.5)	−7.4 (−8.4 to −6.4)	−1.7 (−2.9 to −0.4)
IAP, mmHg	7.5 ± 5.5	12.4 ± 6.9	16.0 ± 6.2	−4.9 (−7.6 to −2.1)	−7.7 (−9.0 to −6.4)	−2.6 (−6.1 to 1.0)

Mean differences and 95% CI were calculated between paired values; $n = 14$. CI, confidence interval; CL, lung compliance; CP, crossing-point between collapse and hyperdistention; CRS, respiratory system compliance; IAP, intra-abdominal pressure; PEEP, positive end-expiratory pressure.

Table 2. *Respiratory mechanics parameters in animals with lung injury*

Parameter	Unloaded	Abdominal Load	Abdominal + Chest Load	Estimated Mean Difference (95% CI)		
				Unloaded vs. Abdominal Load	Unloaded vs. Abdominal + Chest Load	Abdominal vs. Abdominal + Chest Load
Best-PEEP, cmH_2O	11.5 ± 3.2	15.8 ± 3.1	17.2 ± 2.5	−4.5 (−5.1 to −3.6)	−5.7 (−6.7 to −4.6)	−1.3 (−2.2 to −0.5)
Best-C_{RS}, mL/cmH_2O	20.6 ± 3.4	17.7 ± 3.0	14.2 ± 2.8	2.9 (1.6 to 4.2)	6.3 (5.0 to 7.7)	3.4 (2.4 to 4.4)
C_{RS} PEEP3, mL/cmH_2O	14.5 [9.5–16.0]	9.5 [8.0–11.0]	8.5 [7.0–9.0]	3.9 (2.3 to 5.5)	5.4 (3.8 to 7.0)	1.5 (0.8 to 2.2)
Best-C_L, mL/cmH_2O	26.3 ± 5.6	20.3 ± 4.3	16.2 ± 4.1	6.0 (4.1 to 7.9)	10.1 (8.2 to 12.0)	4.1 (2.9 to 5.3)
C_L PEEP3, mL/cmH_2O	17.0 [14.0–22.5]	9.5 [8.0–11.0]	9.5 [8.0–11.0]	7.8 (4.4 to 11.1)	9.0 (5.4 to 12.6)	1.0 (−0.3 to 2.3)
Best-$PEEP_{CP}$, mL/cmH_2O	10.0 [7.5–13.0]	14.0 [14.0–18.0]	18.0 [15.0–18.0]	−4.9 (−6.1 to −3.7)	−6.1 (−7.3 to −4.9)	−1 (−1.9 to −0.1)
IAP, mmHg	7.3 ± 5.5	13.0 ± 5.6	14.6 ± 6.1	−5.7 (−7.1 to −4.3)	−7.4 (−8.7 to −6.0)	−1.6 (−2.9 to −0.3)

Mean differences and 95% CI were calculated between paired values; $n = 12$. CI, confidence interval; CL, lung compliance; CP, crossing-point between collapse and hyperdistention; CRS, respiratory system compliance; IAP, intra-abdominal pressure; PEEP, positive end-expiratory pressure.

Airway Closure

We performed low-flow inflations in 11 pigs. Figure 10 shows representative pressure-volume curves (Fig. 10*A*) from an animal with signs of airway closure after lung injury under abdominal and chest wall load conditions. The curve under combined abdominal and chest load shows evidence of earlier inflection and reduced slope, suggestive of airway closure. Airway segmentations of CT scans from the same animal display apparent narrowing and dropout of central airways under combined load as compared with abdominal load and unloaded conditions (Fig. 10*B*). None of the healthy pigs showed signs of complete airway closure. In pigs with lung injury, complete airway closure was suspected in 2 out of 11 (18%) without loading, in 2 out of 11 (18%) with abdominal loading and in 4 out of 11 (37%) with abdominal and chest loading (Supplemental Table S4). The range of opening pressures among animals with signs of airway closure was 13.6–23.8 cmH_2O. Respiratory mechanics parameters after adjustment for opening pressure are shown in Supplemental Table S4 and Supplemental Fig. S6.

Electrical Impedance Tomography

In both healthy (Supplemental Fig. S7*A*) and injured lungs (Supplemental Fig. S7*B*), the percentage of collapse was higher under loaded conditions at each PEEP below 16 cmH_2O. Collapse was significantly higher in combined abdominal and chest loading than abdominal loading alone at PEEP 10 (healthy) and 14 (injured) cmH_2O. Overdistention was lower than unloaded when loads were applied in both healthy and injured lungs (Supplemental Fig. S7, *C* and *D*), with a significant difference between abdominal loading and combined abdominal and chest loading only at the highest PEEP. The crossing point between the percentage of collapse and hyperdistention identified best-PEEP values (best-$PEEP_{CP}$) that increased across loaded conditions, with a similar trend to the

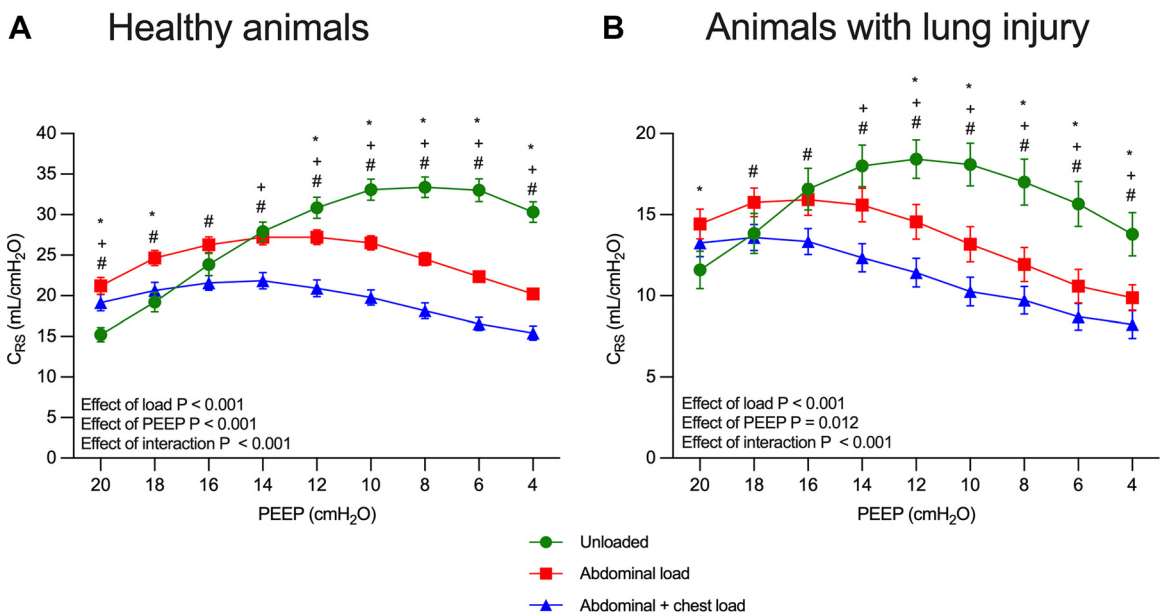

Figure 3. Respiratory system compliance in healthy pigs (*A*) and in pigs with lung injury (*B*). $n = 14$ (healthy animals); $n = 12$ (injured animals); data are presented as means ± SE; *P* for repeated measured ANOVA; green circles indicate the unloaded condition, red squares indicate the abdominal load condition, and blue triangles indicate the combined abdominal + chest load condition; *$P < 0.05$ for comparison between unloaded and abdominal load; +$P < 0.05$ for comparison between unloaded and combined abdominal + chest load; #$P < 0.05$ for comparison between abdominal load and abdominal + chest load. C_{RS}, compliance of the respiratory system; PEEP, positive pressure at end-expiration.

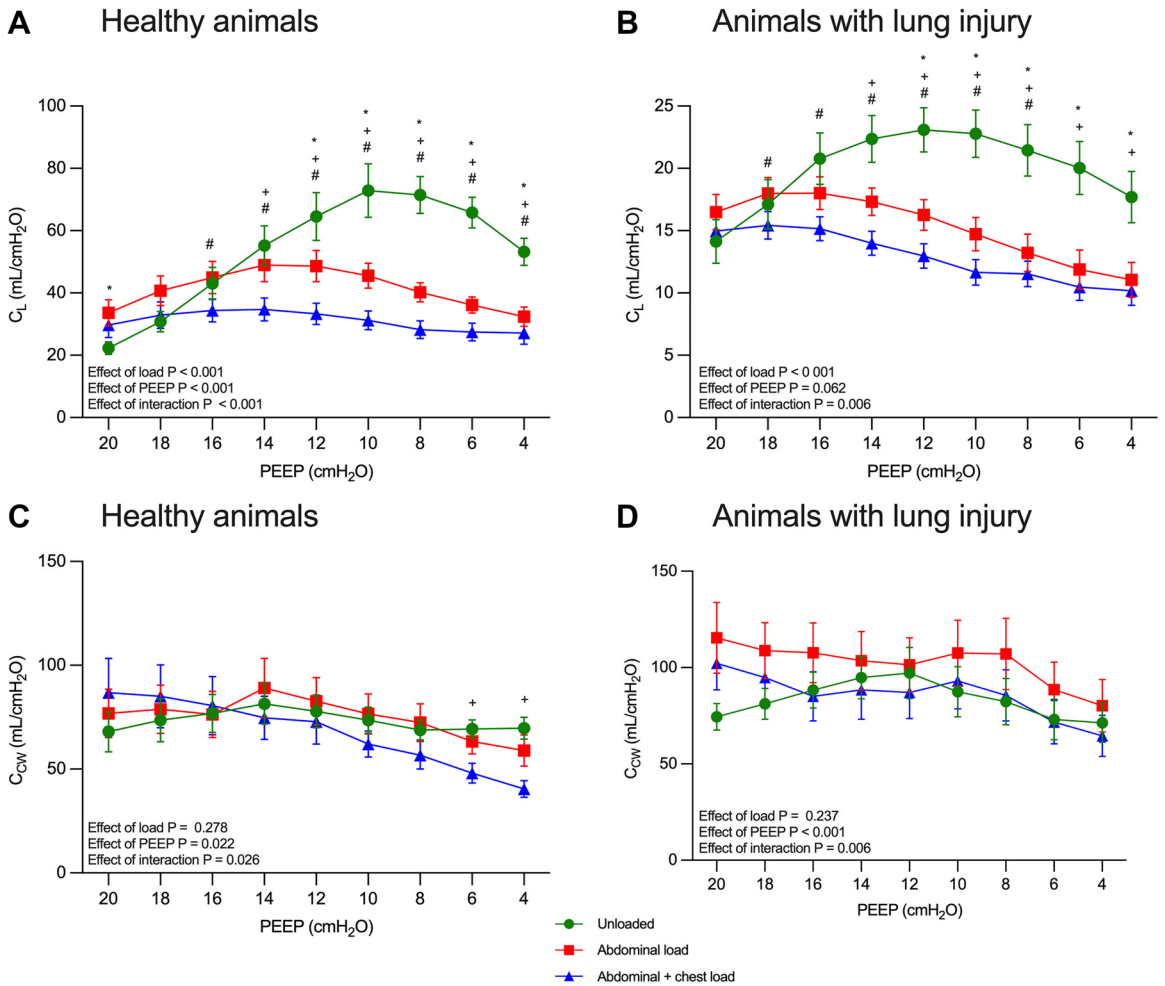

Figure 4. Lung and chest-wall compliance in healthy pigs (*A* and *C*) and in pigs with lung injury (*B* and *D*). $n = 14$ (healthy animals); $n = 12$ (injured animals); data are presented as means ± SE; *P* for repeated measured ANOVA; green circles indicate the unloaded condition, red squares indicate the abdominal load condition, and blue triangles indicate the combined abdominal + chest load condition; $*P < 0.05$ for comparison between unloaded and abdominal load; $+P < 0.05$ for comparison between unloaded and combined abdominal + chest load; $\#P < 0.05$ for comparison between abdominal load and abdominal + chest load. C_{C_W}, compliance of the chest-wall; C_L, compliance of the lung; PEEP, positive pressure at end-expiration.

best-PEEP determined by the highest C_{RS} and with slightly higher values in healthy animals under loaded conditions (Tables 1 and 2).

The main respiratory mechanics and CT variables were also analyzed by stratifying animals by sex. Multiple comparisons showed no significant differences in end-expiratory esophageal pressure and C_{RS} between male and female animals under any of the load conditions, in both healthy and lung injury conditions (Supplemental Fig. S8). Similarly, no sex-related differences were observed in EELV and SP_{global} under either healthy and injured conditions (Supplemental Fig. S9).

DISCUSSION

We replicated the biomechanical effects of excess adiposity in a swine model of AHRF. External mass loading compounded the effects of lung injury on respiratory mechanics and arterial oxygenation. Under mass loading, the best-PEEP could not restore pulmonary compliance and aeration to unloaded values. Chest loading exacerbated the effects of abdominal loading on lung mechanics and geometry. In injured lungs, combined abdominal and chest loading was associated with more frequent airway closure than abdominal-only or unloaded conditions. Overall, these findings may help explain suboptimal responses to PEEP titration in AHRF patients with obesity (15, 16, 35).

Our animal model allowed us to separate the physiological effects of mechanical loading from those of lung injury, which is challenging to achieve in human studies. We identified the best-PEEP using a decremental PEEP trial preceded by a recruitment maneuver. Changes in EELV alone could not fully explain the observed impairment in lung mechanics, suggesting that geometric constraints imposed by elevated mass loading may limit the clinical effectiveness of PEEP optimization. Our findings thus suggest that chest loading may be a key factor promoting airway closure during lung injury.

In our experimental model, applying weights to the abdomen and chest raised intra-abdominal and esophageal pressures to values comparable with those observed in patients with obesity (36) (Tables 1 and 2). As a result, higher PEEP was needed to maintain a positive transpulmonary pressure, as shown in Fig. 2.

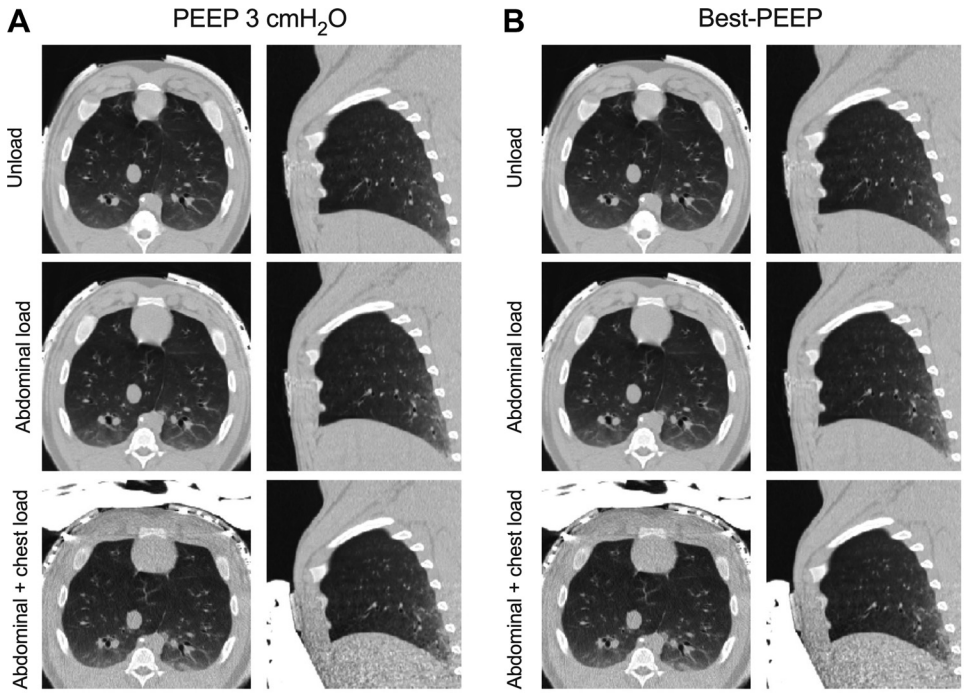

Figure 5. Representative axial and sagittal scans of healthy lungs at PEEP 3 cmH_2O (*A*) and best-PEEP (*B*) across the load conditions. CT images were acquired at end-expiration. CT, computed tomography; PEEP, positive pressure at end-expiration.

Although we did not observe any statistically significant difference in end-expiratory P_{es} between healthy animals and those with lung injury across any of the load conditions, we noted a trend toward lower end-expiratory P_{es} in pigs with lung injury compared with healthy animals (Supplemental Table S3). This counterintuitive finding may be explained by the lower EELV observed in injured lungs relative to healthy ones (Fig. 9 vs. Supplemental Figure S2). At a given PEEP, a decrease in lung volume results in reduced inflation of the chest wall. Since end-expiratory P_{es} reflects the inflation state of the chest wall at end expiration, the reduced EELV would lead to a slightly lower end-expiratory P_{es} in the injured lung. Thus, in our experimental model, the decrease in pleural pressure after lung injury—likely due to reduced lung compliance and the resulting lower lung volumes—may counterbalance the expected increase in pleural pressure caused by increased lung weight (e.g., superimposed pressure).

Under mass loading, C_{RS} decreased due to a reduction in C_L (Figs. 3 and 4). These findings align with observations in ventilated patients with obesity (26, 37), where elevated

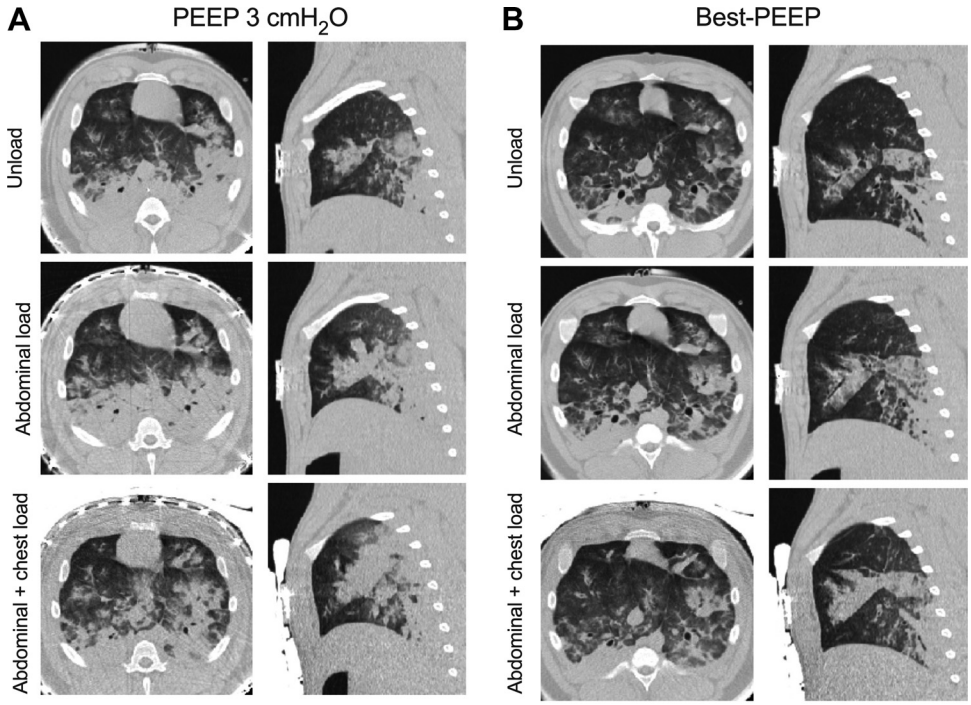

Figure 6. Representative axial and sagittal scans of injured lungs at PEEP 3 cmH_2O (*A*) and best-PEEP (*B*) across the load conditions. CT images were acquired at end-expiration. CT, computed tomography; PEEP, positive pressure at end-expiration.

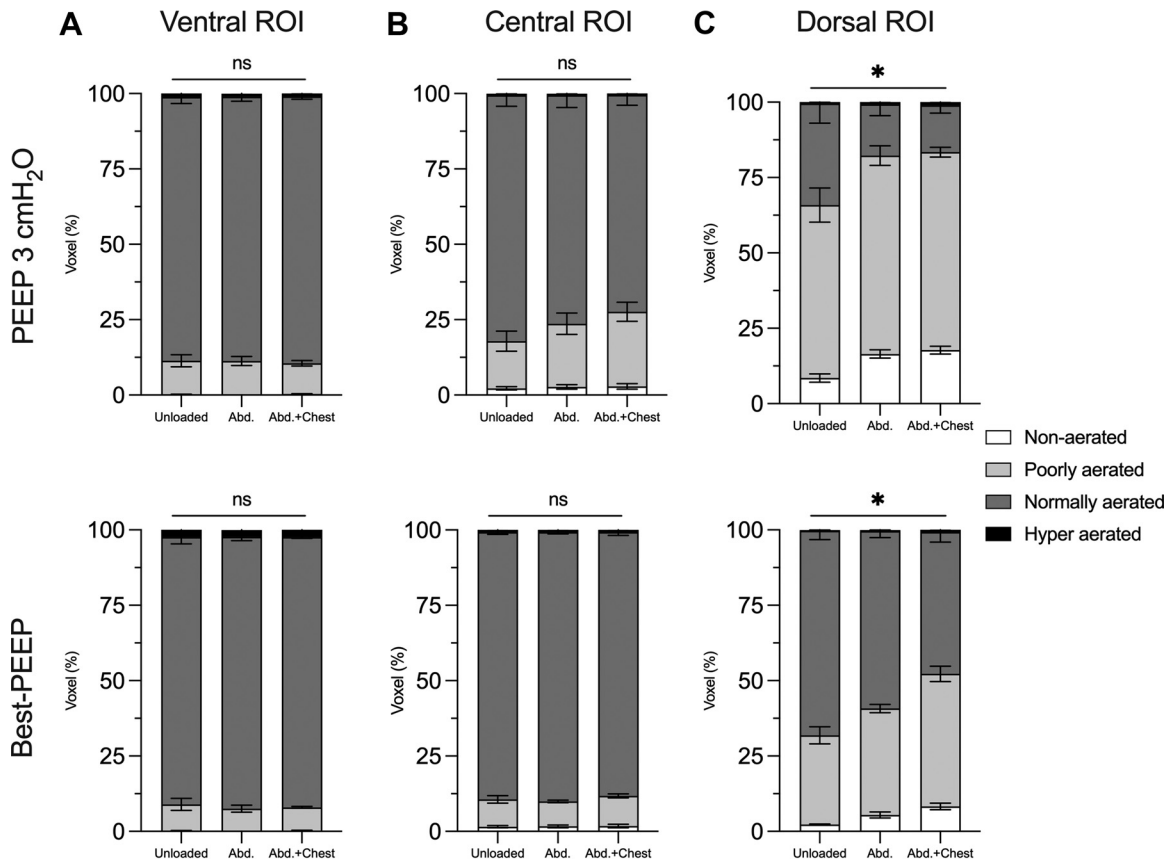

Figure 7. Distribution of nonaerated, poorly aerated, normally aerated, and hyper-aerated voxels in ventral (*A*), central (*B*), and dorsal (*C*) lung regions of interest (ROI) in healthy pigs. $n = 4$; data are presented as means of voxel percentage ± SE; $^*P < 0.05$ for % of nonaerated voxel among load conditions, and ns for non statistically significant, obtained by repeated-measured ANOVA or Friedman test. Abd., presence of abdominal load; Abd. + Chest, presence of combined abdominal and chest load; PEEP, positive pressure at end-expiration.

pleural pressure leads to negative transpulmonary pressure during most of the respiratory cycle. This compressive mechanism reduces lung volumes via pulmonary collapse (7, 16), decreasing C_L and ultimately impairing gas exchange (8, 26, 38) as observed in our animals (Table 2). In the presence of mass loading and lung injury, the decreasing transpulmonary pressure may combine with increased surface tension to increase atelectasis and promote airway closure (28). Overall, the results of the current study illustrate the interactions between mass loading, PEEP, and lung injury on respiratory mechanics.

The best-PEEP increased with load intensity in both healthy and injured pigs. In loaded conditions, the best-PEEP improved EELV, but it did not restore the unloaded values of C_{RS} and C_L. Specifically, the addition of the thoracic load shifted C_{RS} to lower values even when the corresponding EELV values were equivalent, as observed in Fig. 9. This finding suggests that geometric factors beyond lung inflation alone may influence lung mechanics under mass loading. In fact, the addition of thoracic weight decreased both the height and the length of the lungs without affecting their width (Supplemental Figs. S3 and S4). Best-PEEP did not offset the geometric distortion imposed by loading. Because lung expansion occurs anisotropically (39), volume distribution and thus compliance may differ along the three spatial axes. Application of lung restriction along only two axes may therefore uncouple the mechanics of the lungs from their state of overall inflation. Severe obesity alters chest-wall and diaphragm geometry (40), and the lung's adaptation to the shape of the thoracic cavity may influence lung mechanics and response to PEEP. Further supporting the impact of vertical chest constraint on regional lung mechanics, best-PEEP was less effective in recovering nonaerated injured lung in ventral and central lung regions than in dorsal areas, under loaded conditions (Fig. 8). These data suggest that recruitment maneuvers and titrated PEEP may not fully restore aeration in the nondependent lung regions when mass loading is elevated, potentially limiting their efficacy in improving lung mechanics in obesity.

Some previous human studies have shown that best-PEEP can restore pulmonary mechanics to the physiological range (41, 42), whereas others have reported improved pulmonary mechanics without full normalization (16, 35). In a previous study in healthy swine from our group (26), loading was induced by placing saline bags on the lower abdomen. Unlike in the current study, best-PEEP reversed atelectasis and restored lung mechanics, along with total lung volume, to physiological values. This discrepancy may stem from the fact that, in the present study, we distributed sandbags widely over the abdominal and thoracic surfaces, aiming to more closely simulate the effects of mass loading by adipose

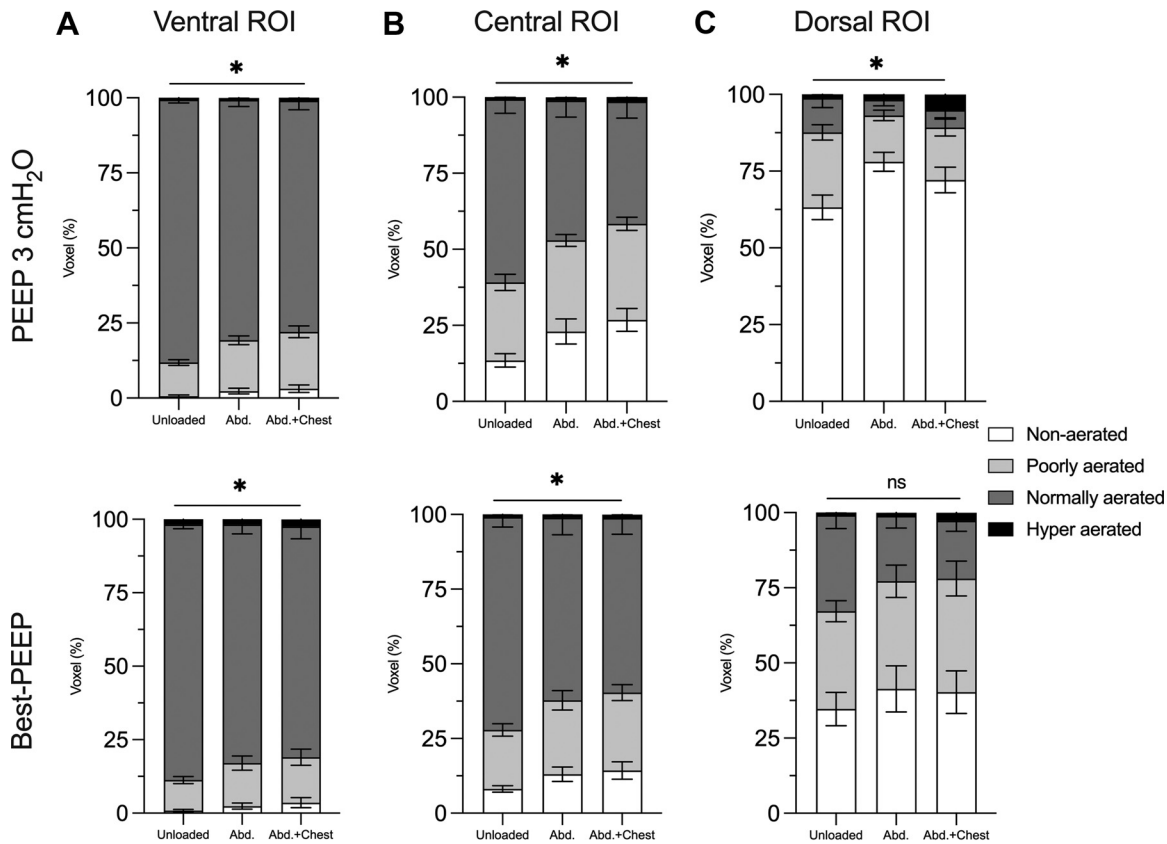

Figure 8. Distribution of nonaerated, poorly aerated, normally aerated, and hyper-aerated voxels in ventral (*A*), central (*B*), and dorsal (*C*) lung ROIs in pigs with lung injury. $n = 7$; data are presented as means of voxel percentage ± SE; $*P < 0.05$ for % of nonaerated voxel among load condition, and ns for non statistically significant, obtained by repeated-measured ANOVA or Friedman Test. Abd., presence of abdominal load; Abd. + Chest, presence of combined abdominal and chest load; PEEP, positive pressure at end-expiration; ROI, region of interest.

tissue (4), resulting in a more widespread distribution of force across the thoracoabdominal surface, rather than creating a focal point of pressure.

The best-PEEP$_{CP}$ determined as the crossing point between percentages of collapse and hyperdistention, as evaluated by EIT, followed a trend similar to the C_{RS}-guided best-PEEP across the load conditions, although small differences were detected in healthy loaded conditions. The percentage of recruitable collapse increased with load, with slightly higher values under combined abdominal and chest loading compared with abdominal loading alone (Supplemental Fig. S7*A*). The loaded condition also exhibited a lower percentage of hyperdistention than without loading (Supplemental Fig. S7*B*), as reported in acute respiratory distress syndrome (ARDS) patients both with and without class III obesity (43). These findings also help explain the crossover pattern of C_{RS} (e.g., higher C_{RS} at unloaded condition at high PEEP level). Unlike previous studies (44, 45), we demonstrated airway closure in a swine model in the present study (Supplemental Table S4; Fig. 10). This was evident only in injured pigs, where the combination of abdominal and chest loading was associated with more airway closure compared with abdominal-only or unloaded conditions. Increased superimposed pressure due to mass loading, coupled with changes in surface tension from lung injury, likely favored airway collapse. In fact, human studies report a higher incidence of airway closure in patients with obesity and ARDS (20, 38). Although we could not localize the site of airway collapse on CT, which resolves airways typically ≥1.5 mm in diameter, we visualized the disappearance of third-generation bronchi during combined abdominal and chest loading, as illustrated in a representative segmented bronchial tree (Fig. 10*B*) from an animal with airway closure. This observation suggests that decreased transmural pressures and thus lower tethering forces of the lung parenchyma on the airway wall led to a smaller airway lumen and shifted the airway segmentation threshold toward more central airways. These smaller luminal diameters may reduce bronchial patency and increase the probability of more distal airway collapse as observed in small animal studies (46) and histological examinations of lungs with ARDS (47). End-expiratory P_{es} did not differ between the loading conditions in injured animals. However, it is likely that chest loading caused more widespread elevation of intrathoracic pressures, affecting both dependent and nondependent regions, whereas end-expiratory P_{es} more accurately reflects pleural pressure in the dependent chest (48).

The application of abdominal and chest loads did not significantly affect chest wall compliance in our study, as shown in Fig. 4. Truncal adiposity might be expected to decrease C_{C_W}, as reported in earlier studies (49). However, recent studies (37, 38) found preserved C_{C_W} in ventilated healthy subjects and AHRF patients with obesity (38), as observed in our animal model. Excess adiposity increases intrathoracic pressure without altering the elastic properties

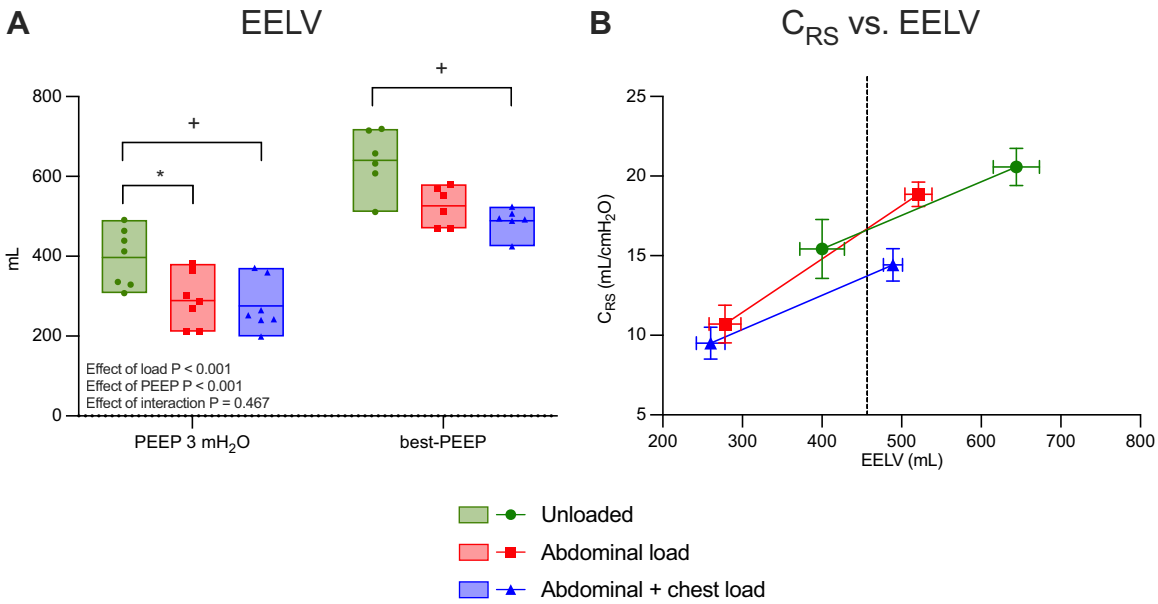

Figure 9. EELV (*A*) and C_{RS} over EELV (*B*) in pigs with lung injury. $n = 7$; data are presented as bars (min. to max., line at mean) (*A*) and as means ± SE (*B*); *P* for repeated measured ANOVA; green bars and green circles indicate the unloaded condition, red bars and red squares indicate the abdominal load condition, blue bars and blue triangles indicate the combined abdominal + chest load condition; $^*P < 0.05$ for comparison between unloaded and abdominal load; $+P < 0.05$ for comparison between unloaded and combined abdominal + chest load. C_{RS}, respiratory system compliance; EELV, end-expiratory lung volume; PEEP, positive pressure at end-expiration.

of the thorax (4, 37), as it shifts the pressure-volume relationship of the chest-wall without affecting its slope (37). This supports mass loading (4) as a mechanism compromising respiratory physiology in obesity and aligns with a recent study from our group, where we found that CT-measured thoracic adiposity correlated with intrathoracic pressure but did not affect C_{C_W} (50). The presence of normal C_{C_W} in obesity implies that, despite lowering peak transpulmonary pressure, mass loading does not protect against tidal lung stretch as the driving pressure applied to the respiratory system is mostly absorbed by the lungs (5). In contrast, elastic loading affects C_{RS} primarily by decreasing C_{C_W} (51–53). In this condition, the higher contribution of the stiffer chest wall to decreasing C_{RS} might have a protective effect on the lungs.

Limitations

The study has important limitations. First, we acknowledge that this simplified model does not recapitulate the complex effects of excess adiposity on inflammatory responses to lung injury and variability in adipose tissue distribution and composition, and their interactions with muscular structures. In particular, increased adiposity around the rib cage, in the mediastinum, and abdominal adiposity leading to excessive thoracic kyphosis and lumbar lordosis, may also influence chest wall compliance, shape, and geometry. However, we developed our model to specifically isolate the biomechanical effects of adiposity on AHRF without the confounding influence of biochemical factors. Furthermore, we believe that under conditions of sedation and complete neuromuscular paralysis, mass loading may represent the primary driver of changes in lung aeration and mechanics. Second, we did not explore the effects of the prone position on lung mechanics and geometry under loading conditions. Third, the anatomy of the swine chest wall, which is triangle-shaped and characterized by elevated stiffness compared with the human chest wall, may dampen the force transmission to the thorax, thereby limiting the effect of chest mass loading. Fourth, esophageal manometry provides an overall estimate of the pleural pressure, primarily reflecting the pleural pressure in the dependent lung. Therefore, we could not investigate the regional changes in pleural pressure under different mass loading configurations. Fifth, we did not investigate the effect of mass loading on lung injuries of varying severity. Therefore, it remains unknown whether a more pronounced lung injury—potentially leading to more severe impairment of gas-exchange, greater tendency toward derecruitment, and more pronounced preexisting airway closure—would amplify synergistic effect with mass loading on lung compliance and aeration, or instead attenuate it. Finally, we performed the same recruitment maneuver for each condition. However, increased intrathoracic pressures across load conditions suggest the transpulmonary pressures during the recruitment maneuver could have been lower for the loaded conditions than for the unloaded condition, possibly affecting the efficacy of alveolar recruitment.

Clinical Implications

In AHRF, the effect of adiposity on respiratory physiology is clinically relevant for several reasons. First, although caution is needed when extrapolating these findings to humans, the failure of titrated PEEP to restore compliance and aeration may underlie ventilator-related morbidity in AHRF patients with obesity. Second, positional therapy may alter lung and airway geometry and affect the response to PEEP. For example, in cases where airway closure is present, the

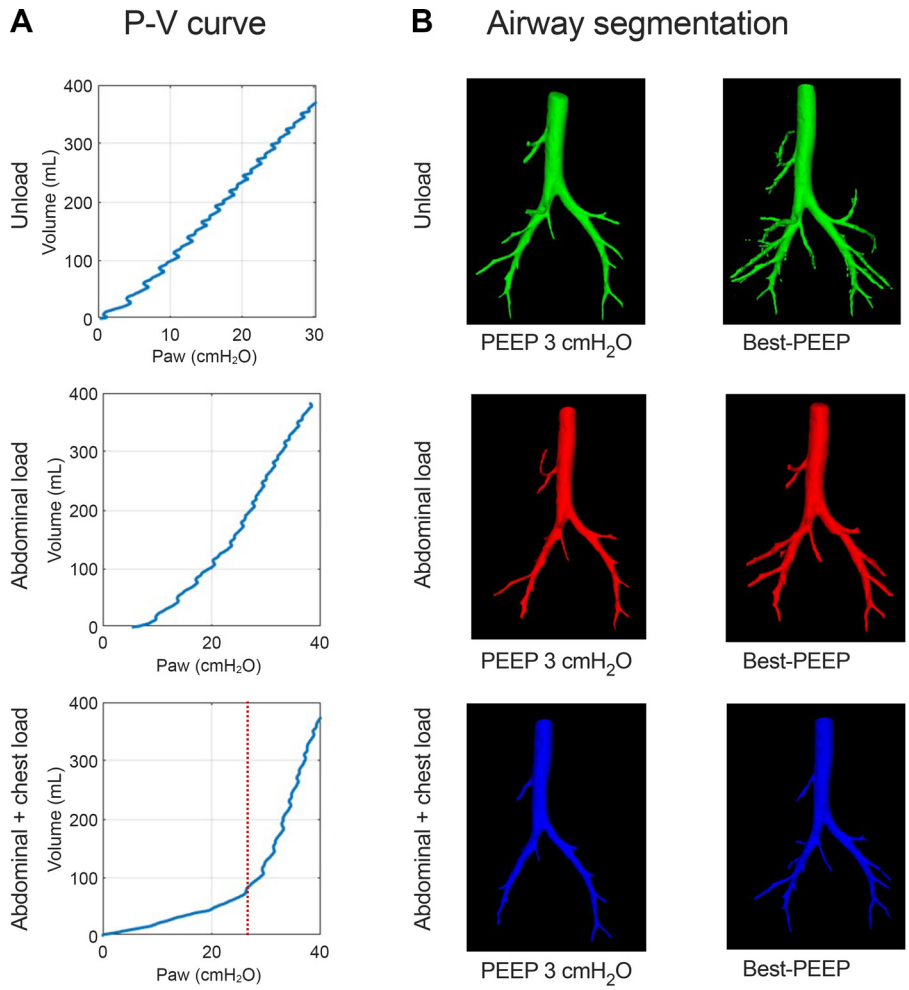

Figure 10. Representative pressure-volume curves during a low flow inflation (*A*) and airway segmentation (*B*) in a pig with lung injury without signs of airway closure in unloaded and abdominal load conditions, and with signs of airway closure in combined abdominal + chest load condition. Red dashed line represents opening pressure. PEEP, positive pressure at end expiration; P-V, pressure-volume.

reverse Trendelenburg position may open distal airways by relieving mass loading and reducing increases intrathoracic pressure (25). Finally, our findings suggest that biometric data, such as waist and hip circumference, could be valuable in identifying patients at higher risk of severe respiratory impairment and airway closure. These patients may benefit from more personalized respiratory care, including advanced respiratory monitoring and early positional therapy.

Conclusions

We developed a controlled physiological model to isolate the mechanical effects of truncal adiposity in AHRF. By demonstrating that, due to geometric constraints, PEEP optimization alone may not restore normal lung mechanics under mass loading, we highlight a mechanistic pathway contributing to PEEP unresponsiveness in obesity. This supports the need for the development of individualized ventilation strategies.

DATA AVAILABILITY

The datasets analyzed for the current study are not publicly available, but are available from the corresponding author on reasonable request.

SUPPLEMENTAL MATERIAL

Supplemental Figs. S1–S9 and Supplemental Tables S1–S4: https://doi.org/10.5281/zenodo.16356083.

GRANTS

This work was funded by the National Institutes of Health (NIH) Grant R01HL137389 (to M.C. and Y.X.) and Grant R01HL171199 (to M.C. and Y.X.).

DISCLOSURES

No conflicts of interest, financial or otherwise, are declared by the authors.

AUTHOR CONTRIBUTIONS

A.N., L.B., M.B.P.A., J.H.T.B., and M.C. conceived and designed research; A.N., Y.X., M.V., T.G.G., G.C.A., S.E.G., R.K., R.G., J.H.T.B., and M.C. performed experiments; A.N., Y.X., M.V., T.G.G., T.W., S.E.G., J.H.T.B., and M.C. analyzed data; A.N., M.V., T.G.G., G.C.A., T.W., R.G., E.R., L.B., M.B.P.A., J.H.T.B., and M.C. interpreted results of experiments; A.N., Y.X., M.V., J.H.T.B., and M.C. prepared figures; A.N., M.V., M.B.P.A., J.H.T.B., and M.C. drafted manuscript; A.N., Y.X., M.V., T.G.G., G.C.A., T.W., S.E.G., R.G., E.R., L.B., M.B.P.A., J.H.T.B., and M.C. edited and revised manuscript; A.N.,

Y.X., M.V., T.G.G., G.C.A., T.W., S.E.G., R.K., R.G., E.R., L.B., M.B.P.A., J.H.T.B., and M.C. approved final version of manuscript.

REFERENCES

1. **Zhi G**, **Xin W**, **Ying W**, **Guohong X**, **Shuying L.** "Obesity paradox" in acute respiratory distress syndrome: asystematic review and meta-analysis. *PLoS One* 11: e0163677, 2016. doi:10.1371/journal.pone.0163677.
2. **Kompaniyets L**, **Goodman AB**, **Belay B**, **Freedman DS**, **Sucosky MS**, **Lange SJ**, **Gundlapalli AV**, **Boehmer TK**, **Blanck HM.** Body mass index and risk for COVID-19–related hospitalization, intensive care unit admission, invasive mechanical ventilation, and death — United States, March–December 2020. *MMWR Morb Mortal Wkly Rep* 70: 355–361, 2021. doi:10.15585/mmwr.mm7010e4.
3. **Bercault N**, **Boulain T**, **Kuteifan K**, **Wolf M**, **Runge I**, **Fleury JC.** Obesity-related excess mortality rate in an adult intensive care unit: a risk-adjusted matched cohort study. *Crit Care Med* 32: 998–1003, 2004. doi:10.1097/01.ccm.0000119422.93413.08.
4. **Sharp JT**, **Henry JP**, **Sweany SK**, **Meadows WR**, **Pietras RJ.** Effects of mass loading the respiratory system in man. *J Appl Physiol* 19: 959–966, 1964. doi:10.1152/jappl.1964.19.5.959.
5. **Grassi L**, **Kacmarek R**, **Berra L.** Ventilatory mechanics in the patient with obesity. *Anesthesiology* 132: 1246–1256, 2020. doi:10.1097/ALN.0000000000003154.
6. **Gaulton TG**, **Berra L**, **Ferreyro BL**, **Cereda M.** Reporting and representation of obesity in randomized controlled trials of noninvasive oxygenation strategies in hypoxemic respiratory failure. *Intern Emerg Med* 17: 2437–2439, 2022. doi:10.1007/s11739-022-03118-2.
7. **Jones RL**, **Nzekwu MM.** The effects of body mass index on lung volumes. *Chest* 130: 827–833, 2006. doi:10.1378/chest.130.3.827.
8. **Pelosi P**, **Croci M**, **Ravagnan I**, **Tredici S**, **Pedoto A**, **Lissoni A**, **Gattinoni L.** The effects of body mass on lung volumes, respiratory mechanics, and gas exchange during general anesthesia. *Anesth Analg* 87: 654–660, 1998. doi:10.1213/00000539-199809000-00031.
9. **Steier J**, **Lunt A**, **Hart N**, **Polkey MI**, **Moxham J.** Observational study of the effect of obesity on lung volumes. *Thorax* 69: 752–759, 2014. doi:10.1136/thoraxjnl-2014-205148.
10. **Derosa S**, **Borges JB**, **Segelsjö M**, **Tannoia A**, **Pellegrini M**, **Larsson A**, **Perchiazzi G**, **Hedenstierna G.** Reabsorption atelectasis in a porcine model of ARDS: regional and temporal effects of airway closure, oxygen, and distending pressure. *J Appl Physiol (1985)* 115: 1464–1473, 2013. doi:10.1152/japplphysiol.00763.2013.
11. **Hedenstierna G**, **Rothen HU.** Respiratory function during anesthesia: effects on gas exchange. *Compr Physiol* 2: 69–96, 2012. doi:10.1002/j.2040-4603.2012.tb00393.x.
12. **Slutsky AS**, **Ranieri VM.** Ventilator-induced lung injury. *N Engl J Med* 369: 2126–2136, 2013. doi:10.1056/NEJMra1208707.
13. **Rezoagli E**, **Laffey JG**, **Bellani G.** Monitoring lung injury severity and ventilation intensity during mechanical ventilation. *Semin Respir Crit Care Med* 43: 346–368, 2022. doi:10.1055/s-0042-1748917.
14. **Webb HH**, **Tierney DF.** Experimental pulmonary edema due to intermittent positive pressure ventilation with high inflation pressures. Protection by positive end-expiratory pressure. *Am Rev Respir Dis* 110: 556–565, 1974. doi:10.1164/arrd.1974.110.5.556.
15. **Fumagalli J**, **Santiago RRS**, **Teggia Droghi M**, **Zhang C**, **Fintelmann FJ**, **Troschel FM**, **Morais CCA**, **Amato MBP**, **Kacmarek RM**, **Berra L**; **Lung Rescue Team Investigators.** Lung recruitment in obese patients with acute respiratory distress syndrome. *Anesthesiology* 130: 791–803, 2019. doi:10.1097/ALN.0000000000002638.
16. **Pirrone M**, **Fisher D**, **Chipman D**, **Imber DA**, **Corona J**, **Mietto C**, **Kacmarek RM**, **Berra L.** Recruitment maneuvers and positive end-expiratory pressure titration in morbidly obese ICU patients. *Crit Care Med* 44: 300–307, 2016. doi:10.1097/CCM.0000000000001387.
17. **Christakoudi S**, **Tsilidis KK**, **Evangelou E**, **Riboli E.** Association of body-shape phenotypes with imaging measures of body composition in the UK Biobank cohort: relevance to colon cancer risk. *BMC Cancer* 21: 1106, 2021. doi:10.1186/s12885-021-08820-6.
18. **Krakauer NY**, **Krakauer JC.** An anthropometric risk index based on combining height, weight, waist, and hip measurements. *J Obes* 2016: 8094275–8094279, 2016. doi:10.1155/2016/8094275.
19. **Krakauer NY**, **Krakauer JC.** A new body shape index predicts mortality hazard independently of body mass index. *PLoS One* 7: e39504, 2012. doi:10.1371/journal.pone.0039504.
20. **Coudroy R**, **Vimpere D**, **Aissaoui N**, **Younan R**, **Bailleul C**, **Couteau-Chardon A**, **Lancelot A**, **Guerot E**, **Chen L**, **Brochard L**, **Diehl J-L.** Prevalence of complete airway closure according to body mass index in acute respiratory distress syndrome. *Anesthesiology* 133: 867–878, 2020. doi:10.1097/ALN.0000000000003444.
21. **Mojoli F**, **Iotti GA**, **Torriglia F**, **Pozzi M**, **Volta CA**, **Bianzina S**, **Braschi A**, **Brochard L.** In vivo calibration of esophageal pressure in the mechanically ventilated patient makes measurements reliable. *Crit Care* 20: 98, 2016. doi:10.1186/s13054-016-1278-5.
22. **Morais CCA**, **Alcala G**, **De Santis Santiago RR**, **Valsecchi C**, **Diaz E**, **Wanderley H**, **Fakhr BS**, **Di Fenza R**, **Gianni S**, **Foote S**, **Chang MG**, **Bittner EA**, **Carroll RW**, **Costa ELV**, **Amato MBP**, **Berra L.** Pronation reveals a heterogeneous response of global and regional respiratory mechanics in patients with acute hypoxemic respiratory failure. *Crit Care Explor* 5: e0983, 2023. doi:10.1097/CCE.0000000000000983.
23. **Baydur A**, **Behrakis PK**, **Zin WA**, **Jaeger M**, **Milic-Emili J.** A simple method for assessing the validity of the esophageal balloon technique. *Am Rev Respir Dis* 126: 788–791, 1982. doi:10.1164/arrd.1982.126.5.788.
24. **Xin Y**, **Martin K**, **Morais CCA**, **Delvecchio P**, **Gerard SE**, **Hamedani H**, **Herrmann J**, **Abate N**, **Lenart A**, **Humayun S**, **Sidhu U**, **Petrov M**, **Reutlinger K**, **Mandelbaum T**, **Duncan I**, **Tustison N**, **Kadlecek S**, **Chatterjee S**, **Gee JC**, **Rizi RR**, **Berra L**, **Cereda M.** Diminishing efficacy of prone positioning with late application in evolving lung injury. *Crit Care Med* 49: e1015–e1024, 2021. doi:10.1097/CCM.0000000000005071.
25. **Grieco DL**, **Anzellotti GM**, **Russo A**, **Bongiovanni F**, **Costantini B**, **D'Indinosante M**, **Varone F**, **Cavallaro F**, **Tortorella L**, **Polidori L**, **Romanò B**, **Gallotta V**, **Dell'Anna AM**, **Sollazzi L**, **Scambia G**, **Conti G**, **Antonelli M.** Airway closure during surgical pneumoperitoneum in obese patients. *Anesthesiology* 131: 58–73, 2019. doi:10.1097/ALN.0000000000002662.
26. **Fumagalli J**, **Berra L**, **Zhang C**, **Pirrone M**, **Santiago RRS**, **Gomes S**, **Magni F**, **Dos Santos GAB**, **Bennett D**, **Torsani V**, **Fisher D**, **Morais C**, **Amato MBP**, **Kacmarek RM.** Transpulmonary pressure describes lung morphology during decremental positive end-expiratory pressure trials in obesity. *Crit Care Med* 45: 1374–1381, 2017. doi:10.1097/CCM.0000000000002460.
27. **Pelosi P**, **Cereda M**, **Foti G**, **Giacomini M**, **Pesenti A.** Alterations of lung and chest wall mechanics in patients with acute lung injury: effects of positive end-expiratory pressure. *Am J Respir Crit Care Med* 152: 531–537, 1995. doi:10.1164/ajrccm.152.2.7633703.
28. **Chen L**, **Del Sorbo L**, **Grieco DL**, **Shklar O**, **Junhasavasdikul D**, **Telias I**, **Fan E**, **Brochard L.** Airway closure in acute respiratory distress syndrome: an underestimated and misinterpreted phenomenon. *Am J Respir Crit Care Med* 197: 132–136, 2018. doi:10.1164/rccm.201702-0388LE.
29. **Gerard SE**, **Patton TJ**, **Christensen GE**, **Bayouth JE**, **Reinhardt JM.** FissureNet: a deep learning approach for pulmonary fissure detection in CT images. *IEEE Trans Med Imaging* 38: 156–166, 2019. doi:10.1109/TMI.2018.2858202.
30. **Gerard SE**, **Herrmann J**, **Kaczka DW**, **Musch G**, **Fernandez-Bustamante A**, **Reinhardt JM.** Multi-resolution convolutional neural networks for fully automated segmentation of acutely injured lungs in multiple species. *Med Image Anal* 60: 101592, 2020. doi:10.1016/j.media.2019.101592.
31. **Gerard SE**, **Herrmann J**, **Xin Y**, **Martin KT**, **Rezoagli E**, **Ippolito D**, **Bellani G**, **Cereda M**, **Guo J**, **Hoffman EA**, **Kaczka DW**, **Reinhardt JM.** CT image segmentation for inflamed and fibrotic lungs using a multi-resolution convolutional neural network. *Sci Rep* 11: 1455, 2021. doi:10.1038/s41598-020-80936-4.
32. **Gattinoni L**, **Caironi P**, **Pelosi P**, **Goodman LR.** what has computed tomography taught us about the acute respiratory distress syndrome? *Am J Respir Crit Care Med* 164: 1701–1711, 2001. Nov 1. doi:10.1164/ajrccm.164.9.2103121.
33. **Costa EL**, **Borges JB**, **Melo A**, **Suarez-Sipmann F**, **Toufen C Jr**, **Bohm SH**, **Amato MB.** Bedside estimation of recruitable alveolar collapse and hyperdistension by electrical impedance tomography. *Intensive Care Med* 35: 1132–1137, 2009. doi:10.1007/s00134-009-1447-y.

34. **Perier F**, **Tuffet S**, **Maraffi T**, **Alcala G**, **Victor M**, **Haudebourg A-F**, **Razazi K**, **De Prost N**, **Amato M**, **Carteaux G**, **Mekontso Dessap A.** Electrical impedance tomography to titrate positive end-expiratory pressure in COVID-19 acute respiratory distress syndrome. *Crit Care* 24: 678, 2020. doi:10.1186/s13054-020-03414-3.
35. **Nestler C**, **Simon P**, **Petroff D**, **Hammermüller S**, **Kamrath D**, **Wolf S**, **Dietrich A**, **Camilo LM**, **Beda A**, **Carvalho AR**, **Giannella-Neto A**, **Reske AW**, **Wrigge H.** Individualized positive end-expiratory pressure in obese patients during general anaesthesia: a randomized controlled clinical trial using electrical impedance tomography. *Br J Anaesth* 119: 1194–1205, 2017. doi:10.1093/bja/aex192.
36. **De Keulenaer BL**, **De Waele JJ**, **Powell B**, **Malbrain ML.** What is normal intra-abdominal pressure and how is it affected by positioning, body mass and positive end-expiratory pressure? *Intensive Care Med* 35: 969–976, 2009. doi:10.1007/s00134-009-1445-0.
37. **Behazin N**, **Jones SB**, **Cohen RI**, **Loring SH.** Respiratory restriction and elevated pleural and esophageal pressures in morbid obesity. *J Appl Physiol (1985)* 108: 212–218, 2010. doi:10.1152/japplphysiol.91356.2008.
38. **Beloncle FM**, **Richard J-C**, **Merdji H**, **Desprez C**, **Pavlovsky B**, **Yvin E**, **Piquilloud L**, **Olivier P-Y**, **Chean D**, **Studer A**, **Courtais A**, **Campfort M**, **Rahmani H**, **Lesimple A**, **Meziani F**, **Mercat A.** Advanced respiratory mechanics assessment in mechanically ventilated obese and non-obese patients with or without acute respiratory distress syndrome. *Crit Care* 27: 343, 2023. doi:10.1186/s13054-023-04623-2.
39. **Hubmayr RD**, **Walters BJ**, **Chevalier PA**, **Rodarte JR**, **Olson LE.** Topographical distribution of regional lung volume in anesthetized dogs. *J Appl Physiol Respir Environ Exerc Physiol* 54: 1048–1056, 1983. doi:10.1152/jappl.1983.54.4.1048.
40. **Boriek AM**, **Lopez MA**, **Velasco C**, **Bakir AA**, **Frolov A**, **Wynd S**, **Babb TG**, **Hanania NA**, **Hoffman EA**, **Sharafkhaneh A.** Obesity modulates diaphragm curvature in subjects with and without COPD. *Am J Physiol Regul Integr Comp Physiol* 313: R620–R629, 2017. doi:10.1152/ajpregu.00173.2017.
41. **Li X**, **Liu H**, **Wang J**, **Ni ZL**, **Liu ZX**, **Jiao JL**, **Han Y**, **Cao JL.** Individualized positive end-expiratory pressure on postoperative atelectasis in patients with obesity: a randomized controlled clinical Trial. *Anesthesiology* 139: 262–273, 2023. doi:10.1097/ALN.0000000000004603.
42. **Wang ZY**, **Ye SS**, **Fan Y**, **Shi CY**, **Wu HF**, **Miao CH**, **Zhou D.** Individualized positive end-expiratory pressure with and without recruitment maneuvers in obese patients during bariatric surgery. *Kaohsiung J Med Sci* 38: 858–868, 2022. doi:10.1002/kjm2.12576.
43. **De Santis Santiago R**, **Teggia Droghi M**, **Fumagalli J**, **Marrazzo F**, **Florio G**, **Grassi LG**, **Gomes S**, **Morais CCA**, **Ramos OPS**, **Bottiroli M**, **Pinciroli R**, **Imber DA**, **Bagchi A**, **Shelton K**, **Sonny A**, **Bittner EA**, **Amato MBP**, **Kacmarek RM**, **Berra L**; **Lung Rescue Team Investigators.** High pleural pressure prevents alveolar overdistension and hemodynamic collapse in acute respiratory distress syndrome with class III obesity. a clinical trial. *Am J Respir Crit Care Med* 203: 575–584, 2021. doi:10.1164/rccm.201909-1687OC.
44. **Martynowicz MA**, **Minor TA**, **Walters BJ**, **Hubmayr RD.** Regional expansion of oleic acid–injured lungs. *Am J Respir Crit Care Med* 160: 250–258, 1999. doi:10.1164/ajrccm.160.1.9808101.
45. **Guérin C**, **Levrat A**, **Pontier S**, **Annat G.** A study of experimental acute lung injury in pigs on zero end-expiratory pressure. *Vet Anaesth Analg* 35: 122–131, 2008. doi:10.1111/j.1467-2995.2007.00363.x.
46. **Broche L**, **Pisa P**, **Porra L**, **Degrugilliers L**, **Bravin A**, **Pellegrini M**, **Borges JB**, **Perchiazzi G**, **Larsson A**, **Hedenstierna G**, **Bayat S.** Individual airway closure characterized in vivo by phase-contrast ct imaging in injured rabbit lung. *Crit Care Med* 47: e774–e781, 2019. doi:10.1097/CCM.0000000000003838.
47. **Rouby JJ**, **Lherm T**, **Martin de Lassale E**, **Poète P**, **Bodin L**, **Finet JF**, **Callard P**, **Viars P.** Histologic aspects of pulmonary barotrauma in critically ill patients with acute respiratory failure. *Intensive Care Med* 19: 383–389, 1993. doi:10.1007/BF01724877.
48. **Yoshida T**, **Amato MBP**, **Grieco DL**, **Chen L**, **Lima CAS**, **Roldan R**, **Morais CCA**, **Gomes S**, **Costa ELV**, **Cardoso PFG**, **Charbonney E**, **Richard JM**, **Brochard L**, **Kavanagh BP.** Esophageal manometry and regional transpulmonary pressure in lung injury. *Am J Respir Crit Care Med* 197: 1018–1026, 2018. doi:10.1164/rccm.201709-1806OC.
49. **Pelosi P**, **Croci M**, **Ravagnan I**, **Vicardi P**, **Gattinoni L.** Total respiratory system, lung, and chest wall mechanics in sedated-paralyzed postoperative morbidly obese patients. *Chest* 109: 144–151, 1996. doi:10.1378/chest.109.1.144.
50. **Spina S**, **Mantz L**, **Xin Y**, **Moscho DC**, **Ribeiro De Santis Santiago R**, **Grassi L**, **Nova A**, **Gerard SE**, **Bittner EA**, **Fintelmann FJ**, **Berra L**, **Cereda M.** The pleural gradient does not reflect the superimposed pressure in patients with class III obesity. *Crit Care* 28: 306, 2024. doi:10.1186/s13054-024-05097-6.
51. **Baydur A**, **Swank SM**, **Stiles CM**, **Sassoon CS.** Respiratory mechanics in anesthetized young patients with kyphoscoliosis. *Chest* 97: 1157–1164, 1990. doi:10.1378/chest.97.5.1157.
52. **Bergofsky EH.** Respiratory failure in disorders of the thoracic cage. *Am Rev Respir Dis* 119: 643–669, 1979. doi:10.1164/arrd.1979.119.4.643.
53. **Sinha R**, **Bergofsky EH.** Prolonged alteration of lung mechanics in kyphoscoliosis by positive pressure hyperinflation. *Am Rev Respir Dis* 106: 47–57, 1972. doi:10.1164/arrd.1972.106.1.47.